Ambient nitrogen reduction cycle using a hybrid inorganic–biological system

Chong Liu[a,b,1], Kelsey K. Sakimoto[a,c,1], Brendan C. Colón[c], Pamela A. Silver[c,2], and Daniel G. Nocera[a,2]

[a]Department of Chemistry and Chemical Biology, Harvard University, Cambridge, MA 02138; [b]Division of Chemistry and Biological Chemistry, School of Physical and Mathematical Sciences, Nanyang Technological University, Singapore, 637371; and [c]Department of Systems Biology, Harvard Medical School, Boston, MA 02115

Contributed by Daniel G. Nocera, May 2, 2017 (sent for review April 17, 2017; reviewed by Shelley D. Minteer and Markus W. Ribbe)

We demonstrate the synthesis of NH_3 from N_2 and H_2O at ambient conditions in a single reactor by coupling hydrogen generation from catalytic water splitting to a H_2-oxidizing bacterium *Xanthobacter autotrophicus*, which performs N_2 and CO_2 reduction to solid biomass. Living cells of *X. autotrophicus* may be directly applied as a biofertilizer to improve growth of radishes, a model crop plant, by up to ∼1,440% in terms of storage root mass. The NH_3 generated from nitrogenase (N_2ase) in *X. autotrophicus* can be diverted from biomass formation to an extracellular ammonia production with the addition of a glutamate synthetase inhibitor. The N_2 reduction reaction proceeds at a low driving force with a turnover number of 9×10^9 cell^{-1} and turnover frequency of 1.9×10^4 s^{-1}·cell^{-1} without the use of sacrificial chemical reagents or carbon feedstocks other than CO_2. This approach can be powered by renewable electricity, enabling the sustainable and selective production of ammonia and biofertilizers in a distributed manner.

nitrogen fixation | *Xanthobacter* | ammonia synthesis | fertilizer | solar

The reduction of N_2 into NH_3 is essential for maintaining the global biogeochemical nitrogen (N) cycle (1). Fixed, organic N in food, biomass, and waste is eventually returned to the atmosphere as N_2 through biological denitrification. As a ubiquitous, synthetic nitrogenous fertilizer, NH_3 synthesized from atmospheric N_2 via the Haber–Bosch process has been added to agricultural soils to drive global increases in crop yields (2). Despite its high efficiency and scalability, the Haber–Bosch process unsustainably employs natural gas as a H_2 feedstock, operates at high temperatures and pressures, and relies on a significant infrastructure for NH_3 distribution (1). A distributed approach toward NH_3 synthesis from renewable energy sources at ambient conditions would enable on-site deployment and reduce CO_2 emissions. To this end, significant effort has been devoted to promoting the reduction of nitrogen to NH_3 with the use of transition metal catalysts (3–5), electrocatalysts (6), photocatalysts (7–11), purified nitrogenases (N_2ases) (11, 12), and heterotrophic diazotrophs (13, 14), potentially powered by renewable energy and operating at ambient conditions. Such approaches, however, typically use sacrificial reductants to drive conversion at low turnover or suffer poor selectivity.

More broadly, the limitations of synthetic NH_3 as a fertilizer have become apparent in recent years as decreasing efficiency of fertilizer use, coupled to environmental damage, has provided an imperative for the development of sustainable biofertilizers (15, 16). Soil microorganisms facilitate efficient nutrient uptake and recycling (17), pathogen resistance (18), environmental adaptation (19), and long-term soil productivity (15). However, the diminished yields of organic/sustainable agriculture have demonstrated that nutrient cycling alone, accentuated by natural variabilities in the soil microbiome, is insufficient to meet an increasing worldwide food demand (20). Attempts to establish robust, productive soil communities through microbial inocula have shown promise (21), but the limited natural flow of organic carbon into these soils results in a bottleneck in the biological activity of these largely heterotrophic biomes (22). An alternative solution would leverage the increasing abundance of renewable energy to cultivate and feed such soil microbiomes, effectively supplementing the natural process of microbial N_2 fixation and plant beneficial interactions.

To further the development of distributed fertilization and natural N cycling, we demonstrate the reduction of N_2 coupled to H_2O oxidation by interfacing biocompatible water-splitting catalysts with the growth of N_2-reducing, autotrophic, biofertilizing microorganisms in a single reactor (Fig. 1). This nitrogen cycle builds on our previous efforts that use H_2 from water splitting to power a bioengineered microorganism to fix CO_2 to biomass and liquid fuels at energy efficiencies far exceeding natural photosynthesis (23, 24). The biocompatible catalysts, a cobalt–phosphorus (Co–P) alloy for the hydrogen evolution reaction (HER) and an oxidic cobalt phosphate (CoP_i) for the oxygen evolution reaction (OER), permit low driving voltages (E_{appl}) under mild conditions (pH 7, 30 °C). The combination of these electrocatalysts with H_2-oxidizing microbes yields CO_2 reduction efficiencies ($\eta_{elec,CO2}$) up to ∼50% (24). The modular design of this renewable synthesis platform may be leveraged beyond fuel production, toward more complex reactions such as the nitrogen reduction reaction (NRR), as well as cultivation of living whole-cell biofertilizers depending on the specific synthetic capabilities

Significance

The nitrogen cycle and the fixation of atmospheric N_2 into ammonium are crucial to global food production. The industrial Haber–Bosch process facilitates half the global nitrogen fixation in the form of ammonia but it is energy- and resource-intensive, using natural gas as the source of energy and hydrogen at elevated temperature and pressure. Our alternative approach synthesizes ammonium from N_2 and H_2O at ambient conditions powered by water splitting, which may be driven renewably. The inorganic–biological hybrid system fixes atmospheric nitrogen into NH_3 or soluble biomass with high fluxes and energy efficiency. Simultaneously, this system cultivates a living soil bacterium that acts as a potent biofertilizer amenable to boosting crop yields.

Author contributions: C.L., K.K.S., B.C.C., P.A.S., and D.G.N. designed research; C.L., K.K.S., and B.C.C. performed research; C.L. and K.K.S. contributed new reagents/analytic tools; C.L., K.K.S., B.C.C., P.A.S., and D.G.N. analyzed data; and C.L., K.K.S., P.A.S., and D.G.N. wrote the paper.

Reviewers: S.D.M., University of Utah; and M.W.R., University of California, Irvine.

Conflict of interest statement: A provisional patent application has been filed related to the technology described in this paper.

Freely available online through the PNAS open access option.

Data deposition: The sequence reported in this paper has been deposited in the National Center for Biotechnology Information Sequence Read Archive (NCBI SRA) database (accession no. SRP073266).

[1]C.L. and K.K.S. contributed equally to this work.

[2]To whom correspondence may be addressed. Email: pamela_silver@hms.harvard.edu or dnocera@fas.harvard.edu.

This article contains supporting information online at www.pnas.org/lookup/suppl/doi:10.1073/pnas.1706371114/-/DCSupplemental.

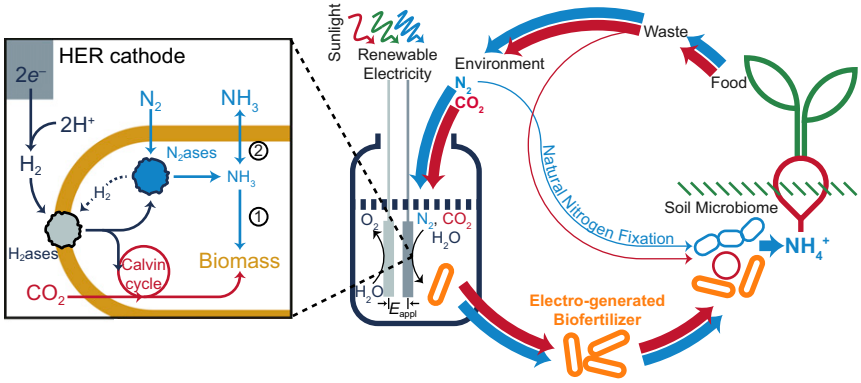

Fig. 1. Schematic of the electroaugmented nitrogen cycle. A constant voltage (E_{appl}) is applied between CoP_i OER and Co–P HER electrodes for water splitting. The H_2ases of *X. autotrophicus* oxidize the generated H_2, fueling CO_2 reduction in the Calvin cycle and N_2 fixation by N_2ases. The generated NH_3 is typically incorporated into biomass (pathway 1), but can also diffuse extracellularly by inhibiting biomass formation (pathway 2). This process is powered by renewable, solar-derived electricity taking N_2 and CO_2 from the environment. Cells of *X. autotrophicus* form an electrogenerated biofertilizer which may be added to soils to improve plant growth. The pathway of natural N cycling/N_2 fixation is indicated, with line width denoting relative flux of these pathways. Red pathways indicate carbon cycling; blue pathways indicate N cycling.

of the microorganism. We exploit this design flexibility to perform the efficient synthesis of NH_3 from N_2 and H_2O by driving the NRR within the H_2-oxidizing, autotrophic microorganism *Xanthobacter autotrophicus*. This Gram-negative diazotrophic bacterium can use H_2 under microaerobic conditions (<5% O_2) as its sole energy source to fix CO_2 and N_2 into biomass (25). We further demonstrate that *X. autotrophicus* functions as a potent electrogenerated biofertilizer, increasing yields of radishes (*Raphanus sativus* L. var. "Cherry Belle"), a fast-growing model food crop.

Results and Discussion

When interfaced with CoP_i | Co–P water-splitting catalysts (Fig. 1), *X. autotrophicus* accumulates fixed N derived from the NRR. An $O_2/CO_2/N_2$ gas mixture (2/20/78) was maintained in the single-chamber reactor housing the Co–P HER cathode and the CoP_i OER anode (*SI Appendix*, Fig. S1). At the beginning of each experiment, *X. autotrophicus* was inoculated into the organic-free, *N*-free minimal medium. A constant driving voltage (E_{appl} = 3.0 V) was applied to the CoP_i | Co–P catalyst system, and aliquots from the reactor were periodically sampled for the quantification of biomass (optical density at 600 nm, OD_{600}) as well as fixed N (detected by two colorimetric assays, *SI Appendix*, Fig. S2*A*). The H_2 generated from water splitting provides the biological energy supply for *X. autotrophicus* to perform the NRR, as well as CO_2 reduction, into biomass without the need for sacrificial reagents (Fig. 2). The amount of faradaic charge passed into water splitting was proportional to biomass accumulation (OD_{600}) as well as the total N content in the medium (N_{total}) during 5-d experiments (Fig. 2*A*). No biofilm formation was observed on either electrode. The fixed N was assimilated into biomass as evidenced by no change in the extracellular soluble N content ($N_{soluble}$). Over the course of the experiment, 72 ± 5 mg L^{-1} of N_{total}, as well as 553 ± 51 mg L^{-1} of dry cell weight accumulated (n = 3, entry 1 in Fig. 2*B* and *SI Appendix*, Table S1). In contrast, no accumulation of N_{total} is observed in controls that omit one of the following elements in our experiment: H_2 from water splitting, *X. autotrophicus*, a single-chamber reactor, or a microaerobic environment (entry 2–5 in Fig. 2*B* and *SI Appendix*, Table S1). The small increases in OD_{600} for entries 4 and 5 in Fig. 2*B* are likely due to light scattering from the accumulation of poly(3-hydroxybutyrate) (PHB). In the dual-chamber experiment where cathode and anode are separated by an anion-exchange membrane (AEM) (entry 4 in Fig. 2*B*), the absence of N_{total} accumulation is concurrent with an increase of soluble Co^{2+} (as determined by inductively coupled plasma mass spectroscopy, ICP-MS) in the medium from 0.9 ± 0.2 μM to 40 ± 6 μM over the course of 24 h, which approaches the ~50-μM half-maximum inhibitory concentration (IC_{50}) of *X. autotrophicus* (*SI Appendix*, Fig. S2*B*). As the AEM is not permeable to cations including Co^{2+}, its use prevents the redeposition of adventitious Co^{2+} onto the CoP_i anode via self-healing, as we have previously described (24, 26), emphasizing the importance of biocompatibility in our system.

Whole-cell acetylene (C_2H_2) reduction (Fig. 2*C*) demonstrated high N_2ase activity in *X. autotrophicus* grown in our hybrid system. This assay provides a measure of the NRR turnover number (TON) by using C_2H_2 as an isoelectronic surrogate of N_2 (25, 27). Aliquots of *X. autotrophicus* sampled directly from our hybrid system reduced C_2H_2 exclusively to C_2H_4 at a rate of 127 ± 33 μM h^{-1} OD_{600}^{-1} (n = 3), when the whole-cell aliquots were incubated under a $C_2H_2/O_2/H_2/CO_2$/Ar gas environment (10/2/9/9/70). The measured C_2H_2-reduction activity corresponds to a rate of N_2 fixation at ~12 mg N_{total} L^{-1}·d^{-1} for cultures of OD_{600} = 1.0, consistent with the measured N_{total} accumulation during the 5-d experiments (entry 1 in Fig. 2*B* and *SI Appendix*, Table S1). Combining a measured cell density of 3.8 ± 0.7 × 10^8 cells mL^{-1}, this C_2H_2-reduction activity translates to an NRR turnover frequency (TOF) of 1.9 × 10^4 s^{-1} per bacterial cell, or roughly ~4 s^{-1}·N_2ase^{-1}, assuming a N_2ase copy number of about 5,000 (28). The similarity between the measured NRR TOF per N_2ase and the values reported in previous studies (12, 27, 29) indicated that the N_2ases are fully functional in our experiments, highlighting the biocompatibility of the water-splitting catalysts in the CoP_i | Co–P | *X. autotrophicus* hybrid system. The equivalent TON is ~9 × 10^9 bacterial $cell^{-1}$ and 2 × 10^6 N_2ase^{-1}, at least two orders of magnitude higher than that previously reported for synthetic (3–5, 7) and biological (11, 29) catalysts (*SI Appendix*, Table S2).

This hybrid system displays high faradaic efficiency for the NRR. A current of 10–12 mA for 100 mL of *X. autotrophicus* culture was needed to maintain sufficient microbial growth. This current was achieved with a cell potential of E_{appl} = 3.0 V (*SI Appendix*, Fig. S2*C*); this high driving voltage is due to the dilute medium salinity as *X. autotrophicus* is sensitive to high salt concentrations (25). The contributions of the HER and the OER overpotentials were determined by examining these half-reactions in the low salinity culture medium. Fig. 2*D* shows the *I–V* characteristics of the Co–P cathode for the HER vs. the normal hydrogen electrode (NHE). A 12-mA current is achieved

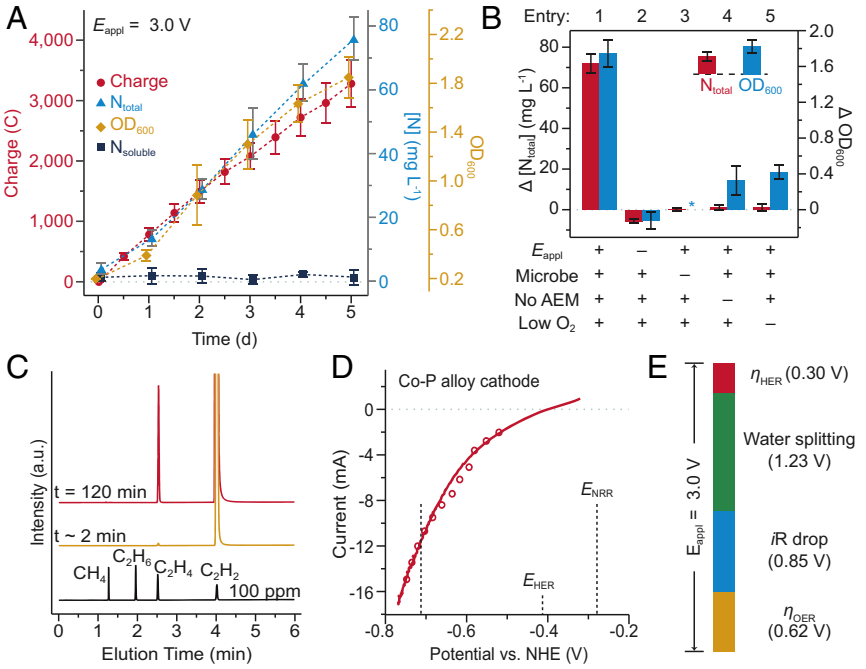

Fig. 2. N_2 reduction on the CoP_i | Co–P | *X. autotrophicus* hybrid system. (*A*) OD_{600}, the amount of charge passed through, the concentration of total N content (N_{total}), and soluble N content ($N_{soluble}$) are plotted versus the duration of experiments. $n \geq 3$; error bars denote SEM. (*B*) Change of N_{total} and OD_{600} under different experimental conditions in 5-d experiments (*SI Appendix*, Table S1). "No AEM" indicates a single-chamber reaction without an anion-exchange membrane. *, not applicable because no bacteria were introduced. $n \geq 3$; error bars denote SEM. (*C*) A qualitative gas chromatography comparison of the whole-cell acetylene reduction with 100-ppm standard sample. *t*, incubation time after C_2H_2 injection. (*D*) Linear scan voltammetry (line, 10 mV s^{-1}) and chronoamperometry (circle, 30-min average) of Co–P HER cathode in *X. autotrophicus* medium, *i*R corrected. The thermodynamic values of HER and NRR (E_{HER}, E_{NRR}) are displayed. (*E*) Contributions of voltage drops within the applied E_{appl} = 3.0 V, as calculated *SI Appendix*. η_{HER} and η_{OER}, overpotentials of HER and OER. a.u., arbitrary units.

for a driving voltage of –0.72 V vs. NHE or at a 0.3-V HER overpotential (η_{HER}) (E_{HER} = –0.41 V at pH = 7). Following a similar procedure for the OER half-reaction, we determined that the OER overpotential (η_{OER}) is 0.62 V. As summarized in Fig. 2*E*, with the measured overpotentials, the contribution of ohmic resistance due to low ionic conductivity is ~28% of E_{appl} (~0.85 V). Given the standard potential difference between the HER and the NRR (E_{HER} = –0.28 V), the driving force for the NRR by *X. autotrophicus* is ~0.43 V, which is lower than the previously reported values that are summarized in *SI Appendix*, Table S2 (3–5, 29, 30). Based on the overall cell potential of 3.0 V, the energy efficiency of NRR ($\eta_{elec,NRR}$) is 1.8 ± 0.3% (n = 3) for a 5-d experiment (*SI Appendix*, Table S1). Parallel to NRR, *X. autotrophicus* fixes CO_2 into cellular biomass (Fig. 2*A*) at a measured $\eta_{elec,CO2}$ = 11.6 ± 1.9% (n = 3). The theoretical value of $\eta_{elec,NRR}$ at E_{appl} = 3.0 V is 7.5 ~11.7% based on the reaction stoichiometry of N_2ase and upstream biochemical pathways. Thus, our observation of $\eta_{elec,NRR}$ = 1.8 ± 0.3% is 15 ~23% of the theoretical $\eta_{elec,NRR}$. The calculated NRR faradaic efficiency is 4.5%, higher than the faradaic efficiencies or quantum yields of other reported NRR systems (6–11) at ambient conditions (*SI Appendix*, Table S2).

Modeling shows that linear microbial growth may be achieved by controlling the H_2 concentration relative to the Michaelis constant of H_2ase (24). Fig. 2*A* shows that linear growth conditions may be achieved for *X. autotrophicus* by balancing the H_2 produced from water splitting and microbial H_2 oxidation. Importantly, the H_2 inhibition constant of N_2ase is $K_i(D_2)$ ~11 kPa (31); the low H_2 partial pressure generated by water splitting (roughly 0.3% or 0.3 kPa H_2, depending on gas flow rate) does not impede N_2 fixation and/or reduce the NRR energy efficiency. When the reactor is pressurized with an external H_2 source, microbial growth is attenuated (*SI Appendix*, Fig. S3*A*). This contention is illustrated by numerical simulations (*SI Appendix*, Fig. S3*B*), which show slower biomass accumulation in the case of microbes under high H_2 concentration but linear growth in CoP_i | Co–P water splitting. In this regard, the direct hybrid device provides potential benefit, as the generated H_2 from water splitting not only provides cellular energy but also controls metabolic pathways, thus allowing growth conditions to be controlled with fidelity.

X. autotrophicus cells can be applied directly to promote plant growth and in this regard is, in effect, a living biofertilizer. Cultures of *X. autotrophicus* were collected, washed, resuspended in 50 mM NaCl saline, and applied to greenhouse radish growth experiments to assess their ability to improve harvest yields (Fig. 3). Increasing amounts of *X. autotrophicus*, applied weekly, increased edible radish storage root mass by up to ~130% compared with unfertilized controls from 3.4 ± 1.2 g plant^{-1} to 8.2 ± 1.4 g plant^{-1} (n = 12 radishes for both) (Fig. 3 *A* and *B* and *SI Appendix*, Fig. S4*A*), and total mass by up to ~100% (*SI Appendix*, Fig. S4 *B* and *C*). To evaluate a potential mechanism of improving plant growth, in vitro fertilization assays were conducted by suspending *X. autotrophicus* cells in a 50 mM NaCl solution and measuring extracellular secretion of N and P. Only living cells of *X. autotrophicus* released NH_4^+ and PO_4^{3-} over the course of the 7-d experiment, with ethanol-killed controls displaying no or negative nutrient release behavior (Fig. 3*C* and *SI Appendix*, Fig. S5 *A* and *B*). Under these saline "starvation" conditions, these bacteria maintained ~50% cell viability, likely metabolizing stored PHB carbon reserves (*SI Appendix*, Fig. S5*A*) (32, 33), demonstrating their capacity to be self-sustaining even in the absence of external energy inputs. Whereas actively growing *X. autotrophicus* cells do not secrete $N_{soluble}$ (Fig. 2*A*), under these starvation conditions, leaky reutilization pathways potentially slowly release N and P from polyglutaminyl-rich cell membranes (34) and polyphosphate granules (32). From this, we contend that living *X. autotrophicus* cells improve plant growth as

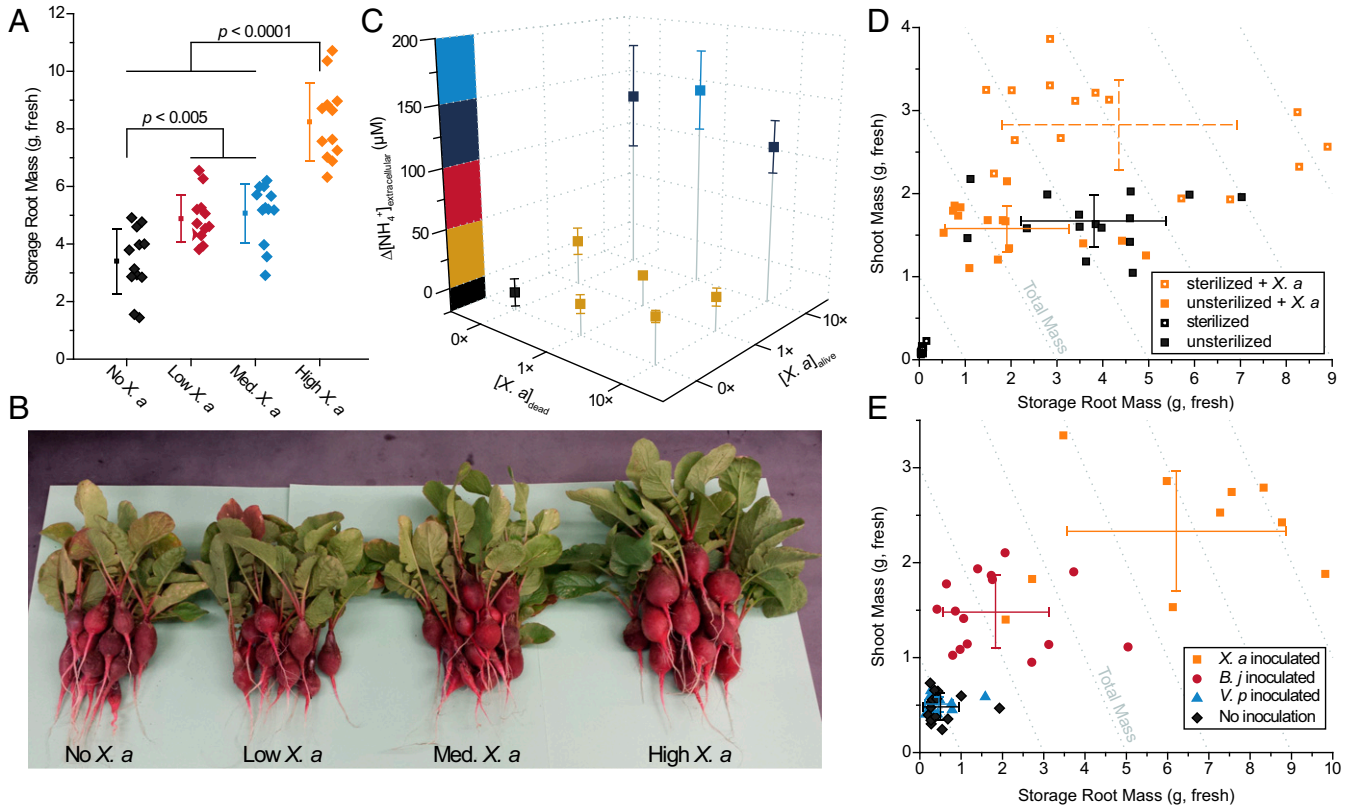

Fig. 3. *X. autotrophicus* biofertilization of radishes. (*A*) Yields of radish storage roots from biofertilization with different amounts of *X. autotrophicus* (*X. a*) (n = 12 radishes per treatment) in as-supplied potting media. No *X. a*: OD_{600} = 0, Low *X. a*: OD_{600} = 0.03, Med. *X. a*: OD_{600} = 0.3, High *X. a*: OD_{600} = 3.0, applied at t = 7, 14 d. Corresponding dry masses and shoot masses are given in *SI Appendix*, Fig. S4 *A*–*C*. Significance (P value) calculated by a two-tailed, heteroscedastic Student's t test. (*B*) Photographs of radishes from *A*. (*C*) Extracellular NH_4^+ release from live and dead *X. autotrophicus* after 7 d in 50 mM NaCl starvation conditions. Dead cells were prepared by 70% EtOH sterilization. 0×: OD_{600} = 0, 1×: OD_{600} = 0.5, 10×: OD_{600} = 5 (n = 3 biological replicates). (*D*) Growth yields of radish seeds with and without seed sterilization by hypochlorite treatment, and preinoculation with and without *X. autotrophicus* (n = 15). Experiments conducted in sterilized potting medium. (*E*) Growth yields of radish seeds sterilized and inoculated with *X. autotrophicus*, *B. japonicum*, *V. paradoxus*, or no inoculation, fertilized at t = 7, 14 d with *X. autotrophicus* biofertilizer in sterilized potting medium. All error bars indicate the SD centered on the arithmetic mean.

a slow-release source of bioavailable N and P, demonstrating the capability of this hybrid inorganic–biological NRR cycle to effectively bridge the gap between atmospheric N_2 and plant biomass.

X. autotrophicus engages in specific plant–microbe and soil microbe–microbe interactions. To study this, we evaluated the effect of soil microbiome composition on *X. autotrophicus* biofertilizer performance. As-supplied potting media (Promix HP MYCORRHIZAE) contains a plant-growth-promoting fungal inoculant. Reuse of the potting media or sterilization by autoclaving effectively removes these microbial species (*SI Appendix*, Fig. S5 *C* and *D*), allowing more direct assessment of radish–*X. autotrophicus* interactions. Interestingly, reused potting media previously fertilized with *X. autotrophicus* exhibit a carryover effect, demonstrating that this biofertilizer improves plant yields over multiple planting cycles (*SI Appendix*, Fig. S5*E*), although comparatively lower yields from cycle 1 to cycle 2 suggest

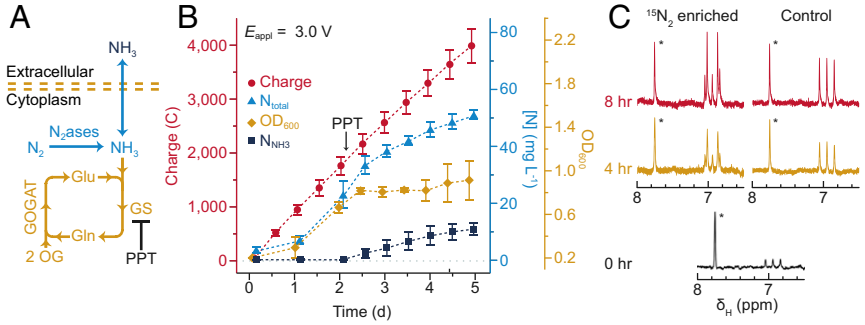

Fig. 4. NH_3 production in the extracellular media. (*A*) Biochemical diagram of NH_3 synthesis from N_2. OG, 2-oxoglutarate; PPT, phosphinothricin. (*B*) The OD_{600}, the amount of charge passed through, the concentration of N_{total} and N_{NH_3} are plotted versus the duration of experiments. The addition of PPT as GS inhibitor was displayed. n = 3; error bars denote SEM. (*C*) The ^{1}H NMR spectrum evolution of generated NH_4^+ under ^{15}N-enriched and naturally abundant N_2. Time counted as the duration after providing $^{15}N_2$. * denotes resonances for the internal standard of H–$CON(CH_3)_2$. Gln, glutamine; Glu, glutamic acid.

continued biofertilization produces the best radish growth. Radish seeds themselves also carry along native microbial inoculants on their seed coat and can be sterilized by quick treatment with a dilute hypochlorite solution (35). Radish seeds sterilized by this method showed lower growth yields (Fig. 3*D*) compared with unsterilized controls, attesting to the importance of plant–microbe commensal interactions. Radish seeds preincubated with *X. autotrophicus* before sowing, in the method of biopriming (35), were able to compensate for the loss of the native radish microbiome, and in fact improve total plant mass by ∼40% compared with unsterilized controls (Fig. 3*D*). This interaction was found to be somewhat specific to *X. autotrophicus* as inoculation of sterilized and unsterilized radish seeds with another diazotroph, *Bradyrhizobium japonicum* [American Type Culture Collection (ATCC) 10324], and a plant-growth-promoting bacterium, *Variovorax paradoxus* (ATCC 17713) (36), showed similar yields as unsterilized radish seeds (*SI Appendix*, Fig. S4*D*). To discern the soil microbe–microbe interactions, radish seeds were inoculated with different plant-growth-promoting bacteria, and fertilized weekly with *X. autotrophicus* cells (Fig. 3*E*). Uninoculated radish seeds in sterile soil showed poor growth even with *X. autotrophicus* fertilization, suggesting that biofertilization is most effective in cooperation with preestablished plant–microbe relationships (from biopriming or soil fungal inoculants) to facilitate nutrient uptake. Growth improved upon inoculation with *B. japonicum* and no significant change was observed with *V. paradoxus*, although the greatest growth increase was for *X. autotrophicus* inoculated and fertilized radishes, at an average storage root mass of 6.2 ± 2.7 g plant^{-1} (n = 10) compared with 0.4 ± 0.2 g plant^{-1} (n = 14) for uninoculated controls, an improvement of ∼1,440%. These results suggest that *X. autotrophicus* not only works as a biofertilizer in conjunction with other members of the soil microbiome (as represented by *B. japonicum*), but that *X. autotrophicus* itself engages in a unique plant-growth-promoting mechanism with radishes to realize increased yields. Its function as a soil and seed inoculant in addition to acting as a N and P source positions it as a potential strategy to revive biologically degraded and nonarable soils (21). Further studies will be required to unambiguously define the mechanism of *X. autotrophicus*–plant interactions.

X. autotrophicus interacts favorably with sustainable abiotic fertilizers. One such natural fertilizer is human urine, which is an attractive alternative soluble N and P fertilizer (37), as well as a potential growth substrate for soil bacteria. *X. autotrophicus* was found to grow autotrophically in a synthetic defined urine medium (38) diluted to an appropriate ionic concentration (*SI Appendix*, Fig. S5*F*). This bacterium was also tolerant to the variable loading of N and P associated with their concentration in natural urine sources (*SI Appendix*, Fig. S5*G*) (39, 40). These results suggest that this biofertilizer is compatible with existing sustainable fertilizers as a potential medium for *X. autotrophicus* cultivation and in-soil propagation. As observed for other soil bacteria (15), the ability of *X. autotrophicus* to transform the labile N and P in urine into stable, slow-release forms is an intriguing prospect for future longitudinal field studies (20).

In addition to fixing N_2 in the form of soluble biomass, the hybrid device can be induced to excrete synthesized NH_3 directly into the extracellular medium. Genome sequencing of the strain of *X. autotrophicus* used here (*SI Appendix*, Table S3) indicates that the NH_3 generated from N_2ase is incorporated into biomass via a two-step process mediated by glutamine synthetase (GS) and glutamate synthase (GOGAT) (Fig. 4*A*), as is consistent with previous biochemical assays (41). If the functionality of this NH_3 assimilation pathway is disrupted, direct production of extracellular NH_3 should occur. Noting that GS inhibitors can induce NH_3 secretion in sugar-fermenting diazotrophs (14), we turned to the specific GS inhibitor phosphinothricin (PPT) (42) to block the NH_3 assimilation pathway and allow NH_3 to passively diffuse out into the extracellular medium (pathway 2 in Figs. 1 and 4*A*). After adding a sufficiently high concentration of phosphinothricin (50 μM) to inhibit GS (42), the biomass accumulation of *X. autotrophicus* slows, while N_{total} and the concentration of free NH_3 in the solution (N_{NH_3}) continues to increase (Fig. 4*B*), indicating that N_2 fixation after phosphinothricin addition is in the form of extracellular NH_3. ^{15}N isotope labeling experiments confirm that the generated NH_3 is from N_2 (Fig. 4*C*). After exposing the microbes to ^{15}N-enriched N_2, the intensity of the $^{15}NH_4^+$ doublet peaks (6.91 ppm, J^1_{NH} = 72.7 Hz) in the ^1H NMR spectrum of the supernatant monotonically increases. This $^{15}NH_4^+$ signal is not detectable in control samples under N_2 of natural abundance; the ^1H NMR exhibits only the triplet signal of $^{14}NH_4^+$ (6.95 ppm, J^1_{NH} = 50.0 Hz). The concentration of N in NH_3 (N_{NH_3}) after terminating the experiment was 11 ± 2 mg L^{-1} (∼0.8 mM) and the accumulated N_{total} reached 47 ± 3 mg L^{-1} (n = 3, *SI Appendix*, Table S1). The rate of N_2 fixation decreases in the latter phase of experiment due to down-regulation at transcriptional and posttranscriptional levels (43).

Conclusion

We demonstrate herein the synthesis of solid N biomass and NH_3 from N_2, driven by water splitting at appreciable TON and TOF, under ambient conditions. By driving water splitting with solar energy and renewable electricity, the approach can potentially provide a renewable synthesis platform for the NRR. We demonstrate that the production of NH_3 and *X. autotrophicus* biofertilizer allows this hybrid inorganic–biological NRR system to effectively connect atmospheric N_2 to plant biomass. The hybrid inorganic–biological approach illustrated for the NRR may be generalized to a renewable biological and chemical synthesis platform, depending on the biomachinery to which water splitting is coupled.

ACKNOWLEDGMENTS. We thank N. Li for ICP-MS measurement; M. Lewandowski for the acetylene reduction assay; B. Greene for numerical simulation; H. Chung for assistance on genome variant calling; S. Zhang for ^1H NMR; and D. Gygi, S. Hays, C. Lemon, X. Ling, C. Myrvhold, and Y. Song from Harvard University, and X. Ling from Nanyang Technological University for helpful discussions. K.K.S. thanks K. J. Woodruff and the Harvard University Arnold Arboretum for assistance with greenhouse studies. C.L. was supported by a Lee Kuan Yew Postdoctoral Fellowship, K.K.S was supported by a Harvard University Center for the Environment Fellowship, and B.C.C. was supported by a predoctoral fellowship from the National Science Foundation Graduate Research Fellowships Program. P.A.S. acknowledges grant support from the Office of Naval Research Multidisciplinary University Research Initiative Award N00014-11-1-0725 and the Wyss Institute for Biologically Inspired Engineering. P.A.S. and D.G.N. thank the Harvard University Climate Change Solutions Fund and the Campus Sustainability Innovation Fund for support. This work was performed at Harvard University under the support of the First 100 W Project, provided by the TomKat Foundation.

1. Smil V (1999) Detonator of the population explosion. *Nature* 400:415.
2. Tilman D, Cassman KG, Matson PA, Naylor R, Polasky S (2002) Agricultural sustainability and intensive production practices. *Nature* 418:671–677.
3. Yandulov DV, Schrock RR (2003) Catalytic reduction of dinitrogen to ammonia at a single molybdenum center. *Science* 301:76–78.
4. Arashiba K, Miyake Y, Nishibayashi Y (2011) A molybdenum complex bearing PNP-type pincer ligands leads to the catalytic reduction of dinitrogen into ammonia. *Nat Chem* 3:120–125.
5. Anderson JS, Rittle J, Peters JC (2013) Catalytic conversion of nitrogen to ammonia by an iron model complex. *Nature* 501:84–87.
6. Lan R, Irvine JTS, Tao S (2013) Synthesis of ammonia directly from air and water at ambient temperature and pressure. *Sci Rep* 3:1145.
7. Liu J, et al. (2016) Nitrogenase-mimic iron-containing chalcogels for photochemical reduction of dinitrogen to ammonia. *Proc Natl Acad Sci USA* 113:5530–5535.
8. Zhu D, Zhang L, Ruther RE, Hamers RJ (2013) Photo-illuminated diamond as a solid-state source of solvated electrons in water for nitrogen reduction. *Nat Mater* 12:836–841.
9. Oshikiri T, Ueno K, Misawa H (2016) Selective dinitrogen conversion to ammonia using water and visible light through plasmon-induced charge separation. *Angew Chem Int Ed Engl* 55:3942–3946.

10. Ali M, et al. (2016) Nanostructured photoelectrochemical solar cell for nitrogen reduction using plasmon-enhanced black silicon. *Nat Commun* 7:11335.
11. Brown KA, et al. (2016) Light-driven dinitrogen reduction catalyzed by a CdS:nitrogenase MoFe protein biohybrid. *Science* 352:448–450.
12. Milton RD, et al. (2016) Nitrogenase bioelectrocatalysis: Heterogeneous ammonia and hydrogen production by MoFe protein. *Energy Environ Sci* 9:2550–2554.
13. Shanmugam KT, Valentine RC (1975) Microbial production of ammonium ion from nitrogen. *Proc Natl Acad Sci USA* 72:136–139.
14. Ortiz-Marquez JCF, Do Nascimento M, Curatti L (2014) Metabolic engineering of ammonium release for nitrogen-fixing multispecies microbial cell-factories. *Metab Eng* 23:154–164.
15. Chaparro JM, Sheflin AM, Manter DK, Vivanco JM (2012) Manipulating the soil microbiome to increase soil health and plant fertility. *Biol Fertil Soils* 48:489–499.
16. Tilman D, Balzer C, Hill J, Befort BL (2011) Global food demand and the sustainable intensification of agriculture. *Proc Natl Acad Sci USA* 108:20260–20264.
17. Carvalho TLG, Balsemão-Pires E, Saraiva RM, Ferreira PCG, Hemerly AS (2014) Nitrogen signalling in plant interactions with associative and endophytic diazotrophic bacteria. *J Exp Bot* 65:5631–5642.
18. Rudrappa T, Czymmek KJ, Paré PW, Bais HP (2008) Root-secreted malic acid recruits beneficial soil bacteria. *Plant Physiol* 148:1547–1556.
19. Rodriguez RJ, et al. (2008) Stress tolerance in plants via habitat-adapted symbiosis. *ISME J* 2:404–416.
20. Mäder P, et al. (2002) Soil fertility and biodiversity in organic farming. *Science* 296: 1694–1697.
21. Wubs ERJ, van der Putten WH, Bosch M, Bezemer TM (2016) Soil inoculation steers restoration of terrestrial ecosystems. *Nat Plants* 2:16107.
22. Kramer C, Gleixner G (2006) Variable use of plant- and soil-derived carbon by microorganisms in agricultural soils. *Soil Biol Biochem* 38:3267–3278.
23. Torella JP, et al. (2015) Efficient solar-to-fuels production from a hybrid microbial-water-splitting catalyst system. *Proc Natl Acad Sci USA* 112:2337–2342.
24. Liu C, Colón BC, Ziesack M, Silver PA, Nocera DG (2016) Water splitting-biosynthetic system with CO_2 reduction efficiencies exceeding photosynthesis. *Science* 352: 1210–1213.
25. Malik KA, Schlegel HG (1980) Enrichment and isolation of new nitrogen-fixing hydrogen bacteria. *FEMS Microbiol Lett* 8:101–104.
26. Bediako DK, Ullman AM, Nocera DG (2016) Catalytic oxygen evolution by cobalt oxido thin films. *Top Curr Chem* 371:173–213.
27. Hoffman BM, Lukoyanov D, Yang Z-Y, Dean DR, Seefeldt LC (2014) Mechanism of nitrogen fixation by nitrogenase: The next stage. *Chem Rev* 114:4041–4062.
28. Schneider K, et al. (1995) The molybdenum nitrogenase from wild-type *Xanthobacter autotrophicus* exhibits properties reminiscent of alternative nitrogenases. *Eur J Biochem* 230:666–675.
29. Danyal K, et al. (2010) Uncoupling nitrogenase: Catalytic reduction of hydrazine to ammonia by a MoFe protein in the absence of Fe protein-ATP. *J Am Chem Soc* 132: 13197–13199.
30. Kuriyama S, et al. (2014) Catalytic formation of ammonia from molecular dinitrogen by use of dinitrogen-bridged dimolybdenum-dinitrogen complexes bearing PNP-pincer ligands: Remarkable effect of substituent at PNP-pincer ligand. *J Am Chem Soc* 136:9719–9731.
31. Guth JH, Burris RH (1983) Inhibition of nitrogenase-catalyzed NH_3 formation by H_2. *Biochemistry* 22:5111–5122.
32. Wiegel J, Wilke D, Baumgarten J, Opitz R, Sschlegel HG (1978) Transfer of the nitrogen-fixing hydrogen bacterium *Corynebacterium autotrophicum* Baumgarten et al. to *Xanthobacter* gen. nov. *Int J Syst Bacteriol* 28:573–581.
33. Trainer MA, Charles TC (2006) The role of PHB metabolism in the symbiosis of rhizobia with legumes. *Appl Microbiol Biotechnol* 71:377–386.
34. Kandler O, König H, Wiegel J, Claus D (1983) Occurrence of poly-γ-D-glutamic acid and poly-α-L-Glutamine in the genera *Xanthobacter, Flexithrix, Sporosarcina* and *Planococcus*. *Syst Appl Microbiol* 4:34–41.
35. Mahmood A, Turgay OC, Farooq M, Hayat R (2016) Seed biopriming with plant growth promoting rhizobacteria: A review *FEMS Microbiol Ecol* 92: fiw112 10.1093/femsec/fiw112.
36. Satola B, Wübbeler JH, Steinbüchel A (2013) Metabolic characteristics of the species *Variovorax paradoxus*. *Appl Microbiol Biotechnol* 97:541–560.
37. Heinonen-Tanski H, van Wijk-Sijbesma C (2005) Human excreta for plant production. *Bioresour Technol* 96:403–411.
38. Anderson MS, Ewert MK, Keener JF, Wagner SA, eds (2015) *Life Support Baseline Values and Assumptions Document* (NASA, Houston), Tech Rep NASA/TP-2015-218570, Document ID 20150002905.
39. Wydeven T, Golub MA (1990) *Generation Rates and Chemical Compositions of Waste Streams in a Typical Crewed Space Habitat* (NASA, Moffett Field, CA), Tech Rep NASA/TM-102799, Document ID 19900019017.
40. Rose C, Parker A, Jefferson B, Cartmell E (2015) The characterization of feces and urine: A review of the literature to inform advanced treatment technology. *Crit Rev Environ Sci Technol* 45:1827–1879.
41. Murrell JC, Lidstrom ME (1983) Nitrogen metabolism in *Xanthobacter* H4-14. *Arch Microbiol* 136:219–221.
42. Gill HS, Eisenberg D (2001) The crystal structure of phosphinothricin in the active site of glutamine synthetase illuminates the mechanism of enzymatic inhibition. *Biochemistry* 40:1903–1912.
43. Dixon R, Kahn D (2004) Genetic regulation of biological nitrogen fixation. *Nat Rev Microbiol* 2:621–631.